Unravelling dispersion forces in liquid-phase enantioseparation. Part II: Planar chiral 1-(iodoethynyl)-3-arylferrocenes

Barbara Sechi, Nutsa Tsetskhladze, Luke Connell, Alessandro Dessì, Roberto Dallocchio, Bezhan Chankvetadze, Sergio Cossu, Tamar Khatiashvili, Victor Mamane, Paola Peluso

Analytica Chimica Acta 1327 (2024) 343160

Contents lists available at ScienceDirect

Analytica Chimica Acta

journal homepage: www.elsevier.com/locate/aca

Unravelling dispersion forces in liquid-phase enantioseparation. Part II: Planar chiral 1-(iodoethynyl)-3-arylferrocenes

Barbara Sechi [a], Nutsa Tsetskhladze [b], Luke Connell [c], Alessandro Dessì [a], Roberto Dallocchio [a], Bezhan Chankvetadze [b], Sergio Cossu [d], Tamar Khatiashvili [b], Victor Mamane [c,**], Paola Peluso [a,*]

[a] Istituto di Chimica Biomolecolare ICB-CNR, Sede secondaria di Sassari, Traversa La Crucca 3, Regione Baldinca, Li Punti, 07100, Sassari, Italy
[b] Institute of Physical and Analytical Chemistry, School of Exact and Natural Sciences, Tbilisi State University, Chavchavadze Ave 3, 0179, Tbilisi, Georgia
[c] Institut de Chimie de Strasbourg, UMR CNRS 7177, Equipe CLIC, 1 rue Blaise Pascal, 67008, Strasbourg Cedex, France
[d] Dipartimento di Scienze Molecolari e Nanosistemi DSMN, Università Ca' Foscari Venezia, Via Torino 155, I-30172, Mestre Venezia, Italy

GRAPHICAL ABSTRACT

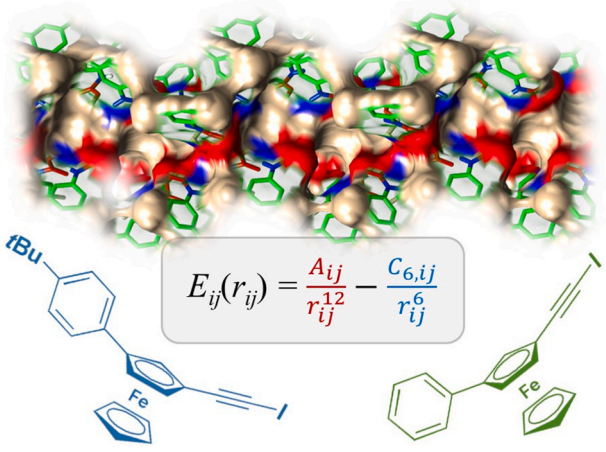

ARTICLE INFO

Keywords:
Dispersion forces
Enantioseparation
High-performance liquid chromatography
Planar chiral ferrocenes
Polysaccharide-based chiral stationary phases

ABSTRACT

Background: In the first part of our study on possible contribution of dispersion forces in liquid-phase enantioseparations, the enantioseparation of the axially chiral 3,3′-dibromo-5,5′-bis-ferrocenylethynyl-4,4′-bipyridine with an amylose *tris*(3,5-dimethylphenylcarbamate)-based chiral column appeared reasonably consistent with a picture of the enantioselective recognition based on the interplay between hydrogen bond (HB), π-π stacking and dispersion interactions.
Results: In the second part of this study, we evaluated the impact of analyte and chiral stationary phase (CSP) structure, mobile phase and temperature on the enantioseparations of planar chiral 1-(iodoethynyl)-3-

* Corresponding author.
** Corresponding author.
E-mail addresses: vmamane@unistra.fr (V. Mamane), paola.peluso@cnr.it (P. Peluso).

https://doi.org/10.1016/j.aca.2024.343160
Received 16 May 2024; Received in revised form 28 July 2024; Accepted 26 August 2024
Available online 27 August 2024

arylferrocenes (3-aryl = phenyl, 2-naphthyl, 4-methylphenyl, 4-*t*-butylphenyl) with polysaccharide-based chiral columns. The main aim of the present study was to understand the molecular bases of the high affinity observed for the second eluted (R_p)-enantiomer of some of these analytes toward amylose phenylcarbamate-based selectors when methanol-containing mixtures were used as mobile phases. Significantly, higher affinity of the second eluted (R_p)-enantiomer toward the selector could be also observed for the sterically hindered 1-(iodoethynyl)-3-(4-*t*-butylphenyl)ferrocene (k_2 = 6.21) compared to the smaller 1-(iodoethynyl)-3-(4-methylphenyl) ferrocenes (k_2 = 4.07) as 2.5% methanol was added to the *n*-hexane-based mobile phase.

Significance: This study reasonably showed that the contribution of dispersion forces may explain the unusually large retention of the second eluted enantiomers observed for the enantioseparation of some planar chiral 1-(iodoethynyl)-3-arylferrocenes with amylose-based selectors. Based on the obtained results, we can conclude that in liquid-phase enantioseparation steric repulsion can be turned into attraction depending on the features of analyte, selector, and mobile phase.

1. Introduction

Elucidating noncovalent interactions play a key role to decipher mechanisms underlying chemical and biological processes [1]. In enantioseparation science, understanding of noncovalent interaction mechanisms has driven the development of efficient chiral selectors and chiral stationary phases (CSPs, chiral selector + stationary phase) to separate the enantiomers of chiral compounds [2]. Furthermore, this knowledge may allow scientists to rationally approach method development at analytical level if mechanisms and noncovalent interactions participating in analyte-chiral selector binding and enantiorecognition are known [3–5]. Among the chiral columns commercially available for high-performance liquid chromatography (HPLC) separation of enantiomers, those based on polysaccharide phenylcarbamates as chiral selectors are the most popular and versatile. These polymeric selectors feature a highly ordered extended chiral surface, rich in recognition sites, and able to exert multiple noncovalent interactions with analyte enantiomers [6]. In Fig. 1, the structure of amylose *tris*(3,5-dimethylphenylcarbamate) is depicted as a representative example. The amidic hydrogens (blue) and the carbonyl oxygens (red) of the carbamate pendant groups at the 2, 3, and 6 positions of the glucopyranose residues forming the polysaccharide backbone act, respectively, as hydrogen bond (HB) donors and acceptors. HB has a pivotal role in the enantioseparations by polysaccharide phenylcarbamate-based selectors. Indeed, *a*) intramolecular HBs within the polysaccharide derivative, contributing to sustain the high-ordered structure of the polymeric selector, *b*) stereoselective intramolecular HBs within the analyte, determining conformational features of each interacting analyte, and *c*) intermolecular HBs between analyte and selector, sustaining diastereomeric complex formation and differentiation, were found to contribute to binding and recognition [8,9]. The involvement of the carbamate sites in halogen [10], chalcogen, and π-hole bonds [11] was recently demonstrated. Furthermore, π-π interactions are very important noncovalent forces acting in these chiral selectors [12,13].

Amylose carbamates present a more compact structure compared to cellulose-based derivatives. This feature may favour closer contacts between analyte and selector, making amylose carbamates suitable extended surfaces to identify the contribution of dispersion forces in liquid-phase enantioseparation [14]. Often, in amylose-based selectors the enantioseparation results from a fine balance between the advantage of having close contacts between analyte and selector surface [15], and the disadvantage of steric effects opposing to the penetration of large analytes into the compact chiral groove of the selector [16]. Close contacts (attraction) and steric hindrance (repulsion) recall the concept of dispersion (London) forces [17,18]. Indeed, London dispersion corresponds to the attractive part of the van der Waals potential, whereas the 'steric repulsion' is associated to the repulsive part of potential (Fig. 2). Thus, there is a subtle boundary between the two opposing

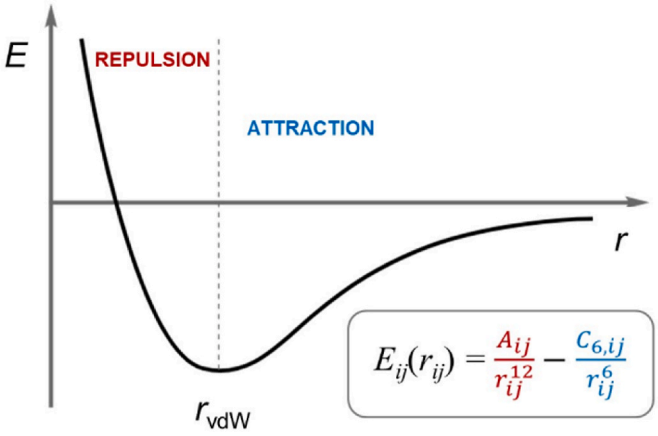

Fig. 2. Repulsive and attractive (dispersion) contribution to van der Waals potential.

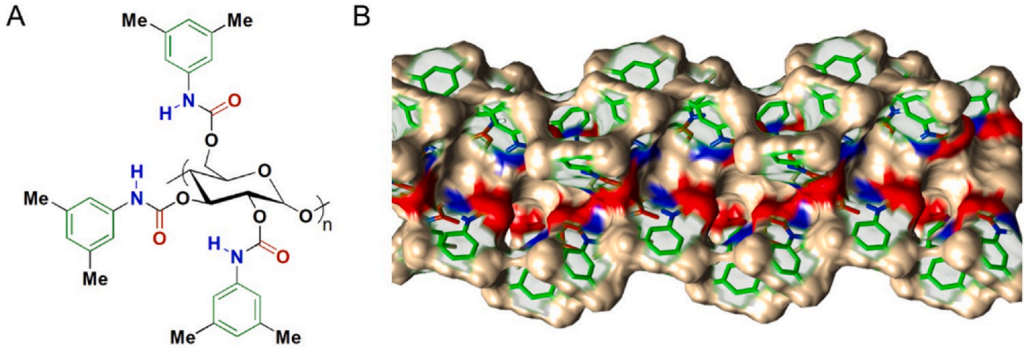

Fig. 1. Amylose *tris*(3,5-dimethylphenylcarbamate): A) drawing structure; B) 12-mer model, graphically generated with the Chimera 1.13.1 software [7] (surface representation over a tube model). Colours: aryl group (green), N–H (blue), C═O (red). (For interpretation of the references to colour in this figure legend, the reader is referred to the Web version of this article.)

forces [19,20]. On the other hand, a strong stabilizing contribution from dispersion forces was often found for noncovalent interactions between neutral, sterically hindered organic molecules. As a matter of fact, this contribution turns the 'steric repulsion' into a 'steric attraction' [21]. Furthermore, the strength of dispersion interactions depends on the size and number of the interacting groups and on their polarizabilities [22]. For instance, dispersion forces were demonstrated to have a relevant role in determining folding of biomacromolecules [23] where, in general, HBs as well as π-π stacking are considered as dominant noncovalent interactions.

Although several studies demonstrated that dispersion forces may control molecular aggregation and may have a relevant role in thermodynamic stability, molecular recognition, chemical selectivity, and many other chemical and biological phenomena, the study of dispersion forces is rather underrepresented in analytical enantioselective recognition. Given that dispersion forces are strongly distance-dependent (given r the distance between two interacting atoms, dispersion attraction is of the order of r^{-6}, see Fig. 2) and that the compact structure of amylose-based chiral selectors may favour closer noncovalent contacts, our hypothesis is that dispersion-type forces may underlie the enantioselective recognition of the planar chiral ferrocenes featuring extended π-electron clouds by using these chiral selectors in HPLC environment. The following remarks supported our starting hypothesis:

1) Unusual enantioseparations were recently reported for compounds **1**–**3** (Table 1), which presented interesting features not directly explainable by invoking HB and/or π-π stacking [14,15,24]. Irrespective of mobile phase type used to elute the enantiomers, at comparable flow rate, these processes shared the following features: *a*) high retention factor for the second eluted enantiomer (k_2) ranging from 23.95 to 52.50; *b*) these large separations were observed on the amylose *tris*(3,5-dimethylphenylcarbamate) as chiral selector; *c*) all analytes featured extended π-electron clouds and contained ferrocene as distinctive structural signature. In this regard, it is worth noting that London dispersion is a purely quantum mechanical effect due to electron correlation and attributed to fluctuating induced dipoles [18]. Based on this view, molecules with high polarizability and featuring extended π-electron system were envisaged as high contributors to dispersion forces [25] and, in this frame, π-conjugated ferrocenes were shown to behave as dispersion energy donors [26].
2) In a previous study [14], the enantioseparation results obtained for compound **1** appeared reasonably consistent with a picture of the enantioselective recognition based on the interplay between HB, π-π stacking and dispersion interactions dependent on analyte structure and features of the polysaccharide surfaces. In this regard, it is worth mentioning that London dispersion was recently found to be an important factor for the stabilization of azobenzene derivatives in the presence of HB [27].
3) An unusual increase of the retention factor of the second eluted (k_2) (R_p)-enantiomers was observed for compound **3** with the amylose *tris* (3,5-dimethylphenylcarbamate)-based chiral column as the mobile phase was changed from *n*-hexane/propan-2-ol (2-PrOH) 95:5 v/v to *n*-hexane/2-PrOH/methanol (MeOH) 95:2.5:2.5 v/v/v [15].
4) In the frame of the present study, we compared *n*-hexane/2-PrOH 90:10 v/v, EtOH and MeOH as mobile phases for the enantioseparation of **1** and **3** with Lux Amylose-1, showing that the dependence of retention and enantioseparation on mobile phase polarity was opposite for the two compounds (Supplementary data, Fig. S1). Indeed, whereas k_2 decreased following the order *n*-hexane/2-PrOH 90:10 v/v ≫ EtOH > MeOH for ferrocene **1**, the opposite trend was observed for ferrocene **3** (MeOH > EtOH ≫ *n*-hexane/2-PrOH 90:10 v/v). This could indicate that if dispersion forces contributed to the high affinity of the second eluted enantiomers in both cases, the contribution of dispersion occurred in different scenarios in terms of noncovalent interaction patterns, dominated in the first case by HB (favoured by *n*-hexane-based mobile phases) and by π-π and hydrophobic interactions (favoured by polar organic solvents like EtOH and MeOH) in the second case.

In this second part of our study on possible contribution of dispersion forces in liquid-phase enantioseparations, we examined the enantioseparation of planar chiral 1-(iodoethynyl)-3-arylferrocenes **3**–**6** (Fig. 3) as follows: a) the impact of analyte structure, chiral selector, mobile phase and temperature on the enantioseparations was evaluated for 1-(iodoethynyl)-3-arylferrocenes **3** and **4** with the aim to understand the molecular bases of the high affinity observed for the second eluted enantiomer (R_p) of these analytes with amylose carbamate-based selectors and dependent on the presence of methanol in the mobile phase

Table 1
Recent high-performance liquid-phase enantioseparations of chiral ferrocene derivatives featuring extended π-electron clouds performed with amylose *tris*(3,5-dimethylphenylcarbamate) as chiral selector (T = 25 °C).

Ferrocene	Chiral column [a]	Mobile phase [b]	*FR* [c]	α [d]	k_2 [e]	EEO [f]	[Ref.]
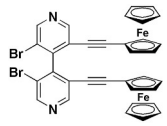 **1**	Lux Amylose-1	*n*-hexane/2-PrOH 90:10	0.8	5.08	31.60	(*M*)-(*P*)	[14]
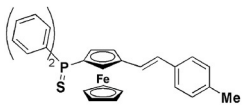 **2**	Chiralpak AD-3	2-PrOH 100 %	1.0	84.68	52.50	(S_p)-(R_p)	[24]
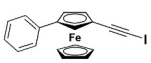 **3**	Lux Amylose-1	MeOH 100 %	0.8	11.41	23.95	(S_p)-(R_p)	[15]

[a] Lux Amylose-1 (Phenomenex), Chiralpak AD-3 (Chiral Technologies).
[b] MeOH, methanol; 2-PrOH, 2-propanol.
[c] *FR*, flow rate.
[d] α, selectivity.
[e] k_2, retention factor of the second eluted enantiomer.
[f] EEO, enantiomer elution order.

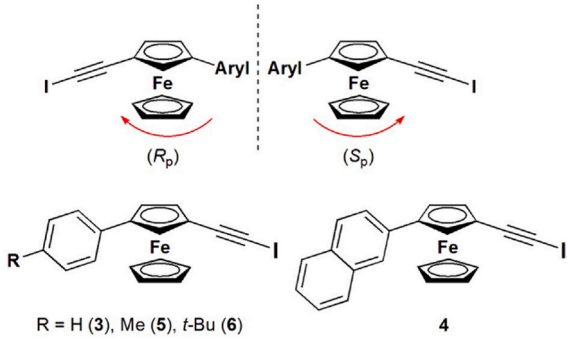

Fig. 3. Structures of planar chiral 1-(iodoethynyl)-3-arylferrocenes **3**–**6**. (R_p)- and (S_p)-enantiomers are also depicted.

[15]; *b*) the enantioseparations of 1-(iodoethynyl)-3-(4-substituted phenyl)ferrocenes **5** (4-substituent = methyl) and **6** (4-substituent = *t*-butyl) with a chiral column based on amylose *tris*(3,5-dimethylphenylcarbamate) were performed and compared to explore the impact of increasing steric hindrance of the analyte on the affinity of the (R_p)-enantiomer toward the amylose-based selector.

The general aim of this study was to understand if in liquid-phase enantioseparation steric repulsion can be turned into dispersion attraction depending on the structural features of analytes and polysaccharide selectors, as well as mobile phase polarity.

2. Materials and methods

2.1. Reagents and chemicals

Compounds *rac*-**3**, *rac*-**4** and their (S_p)-enantiomers were prepared and characterized as previously reported [28]. Compounds *rac*-**5**, *rac*-**6** and their (S_p)-enantiomers were prepared in the frame of this study, and all details on their synthesis and characterization are reported in the Supplementary data. HPLC grade *n*-hexane, MeOH, 2-PrOH, acetonitrile (ACN), and water were purchased from Sigma-Aldrich (Taufkirchen, Germany). Experimental details about X-ray diffraction (XRD) analyses of compounds **5** (Fig. S2) and **6** (Fig. S3) are reported in the Supplementary data.

2.2. Chromatography

An Agilent Technologies (Waldbronn, Germany) 1100 Series HPLC system (high-pressure binary gradient system equipped with a diode-array detector operating at multiple wavelengths [220, 254, 280, and 360 nm], a programmable autosampler with a 20-μl loop, and a thermostated column compartment) was employed. Data acquisition and analyses were carried out with Agilent Technologies ChemStation Version B.04.03 chromatographic data software. The UV absorbance is reported as milliabsorbance units (mAU). Lux Cellulose-1 [cellulose *tris* (3,5-dimethylphenylcarbamate)], Lux i-Cellulose-5 [cellulose *tris*(3,5-dichlorophenylcarbamate)], Lux Amylose-1 and Lux i-Amylose-1 [amylose *tris*(3,5-dimethylphenylcarbamate)], and Lux i-Amylose-3 [amylose *tris*(3-chloro-5-methylphenylcarbamate)] (5 μm) (Phenomenex Inc., Torrance, CA, USA) were used as chiral columns (250 × 4.6 mm) (Supplementary data, Table S1). Analyses were performed in isocratic mode at 25 °C. The flow rate was set at 0.8 ml/min, if not indicated otherwise. Dead time (t_0) was measured by injection of tri-*tert*-butylbenzene (Sigma-Aldrich) as a non-retained compound [29]. The van't Hoff experiments were conducted in the following conditions: *a*) at 5, 10, 15, 20, 25, 30, 35, 40, and 45 °C by using a thermostat jacket equipped with a RE104 Lauda circulating water bath (Lauda, Königshofen, Germany) (resolution 0.1 °C; accuracy ±0.4 °C; temperature control ±0.02 °C); *b*) at 10, 15, 20, 25, 30, 35, 40, 45, 50, 55, 60 °C by using a home-made immobilized amylose *tris*(3,5-dimethylphenylcarbamate)-based chiral column and an Agilent 1200 HPLC instrument (Agilent Technologies, Waldbronn, Germany) equipped with a G1367C HiP ALS-SL autosampler, G1316B TCCSL temperature controller, G1311A quaternary pump and G1314D VWD variable wavelength detector. For these series of analyses, the Chemstation software (version B.03.02-SR2) was used for instrument control, data acquisition and data processing. In all cases, when the temperature was changed, the column was allowed to equilibrate for 1 h before injecting the samples. Thermodynamics parameters were derived from the slopes and the intercepts of the van't Hoff plots by linear regression analysis (see Supplementary data for theory details). Statgraphics Centurion 18 (Statpoint Technologies, Inc., Warrenton, VA, USA) was used for all linear regression analyses. For all analytes, the enantiomer elution order (EEO) was determined by injecting (S_p)-enantiomers prepared by asymmetric syntheses [28] (see Supplementary data for **5** and **6**).

2.3. Computationals

Polarizabilities (α) [atomic unit, au] of ACN (28.75 au), *n*-hexane (72.80 au), MeOH (19.12 au), and water (5.74 au) were calculated by using Gaussian 16W (Wallingford, CT, USA) [30] at DFT level of theory with the B3LYP functional and the 6-31G(d) basis set, applying tight convergence criteria and the solvation model based on density (SMD) as variation of IEFPCM (integral equation formalism for polarizable continuum model) of Truhlar and co-workers [31].

3. Results and discussion

In the present study, we focused on the 1-(iodoethynyl)-3-arylferrocenes, considering and comparing the enantioseparation outcomes of **3** and **4** with different chiral columns and mobile phases. These planar chiral ferrocenes contain aromatic substituents, i.e. 3-aryl = phenyl and 2-naphthyl, respectively. Thus, compound **4**, with the more polarizable 2-naphthyl group, was expected to be a better dispersion energy donor compared to **3**. On the other hand, calculated properties showed electron charge density on the main recognition sites slightly higher for **3** compared to **4** [15]. Furthermore, **4** showed higher steric hindrance compared to **3** and, consequently, the penetration of this compound within the compact structure of the amylose-based chiral selectors could be disfavoured. On these bases, subtle differences for compounds **3** and **4** in terms of enantioseparation outcomes with polysaccharide-based chiral selectors were expected based on the subtle differences observed in terms of electronic and steric effects.

3.1. Enantioseparation of *3* and *4*: an overview on the impact of analyte structure, chiral selector, and mobile phase

In a first screening, the effect of Lux Cellulose-1, Lux i-Cellulose-5, Lux-Amylose-1, Lux i-Amylose-1, and Lux i-Amylose-3 was studied and compared by using *n*-hexane/2-PrOH 90:10 v/v as mobile phase (Fig. 4 and Supplementary data, Table S2 and Fig. S4). The following remarks emerged:

1. *Cellulose-versus amylose-based columns.* Retention factors were higher for **4** compared to **3** with almost all columns, except for i-Amylose-1 and i-Amylose-3 where **3** showed higher k_2 compared to **4.** Whereas for compound **4** the selectivity of enantioseparation was higher on the Cellulose-1 compared to **3**, the opposite was observed with all amylose-based columns. Furthermore, a backbone-dependent reversal of the enantiomer elution order (EEO) was observed for both compounds [(R_p)-(S_p) for Cellulose-1 and (S_p)-(R_p) for Amylose-1, i-Amylose-1, and i-Amylose-3].
2. *Coated versus immobilized columns.* By comparing Amylose-1 and its immobilized version i-Amylose-1, retention factors decreased in almost all cases on the immobilized column, except for k_2 of

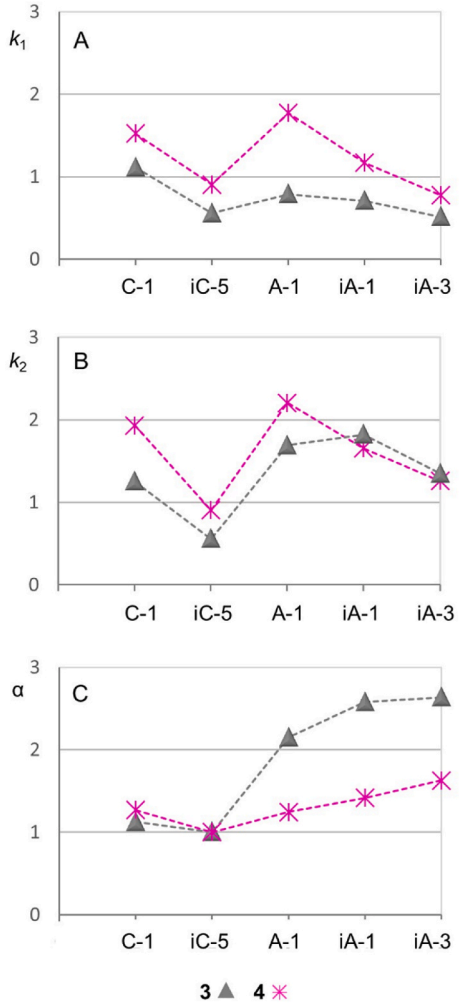

Fig. 4. Comparison of retention factors of first (k_1) (A) and of second (k_2) (B) eluted enantiomers, and selectivity (α) (C) of compounds **3** and **4** on Lux Cellulose-1 (C-1), i-Cellulose-5 (iC-5), Amylose-1 (A-1), i-Amylose-1 (iA-1), and i-Amylose-3 (iA-3) as chiral columns with *n*-hexane/2-propanol 90:10 v/v as mobile phase (flow rate = 0.8 ml/min, T = 25 °C) (for chromatographic parameters see Table S2, Supplementary data).

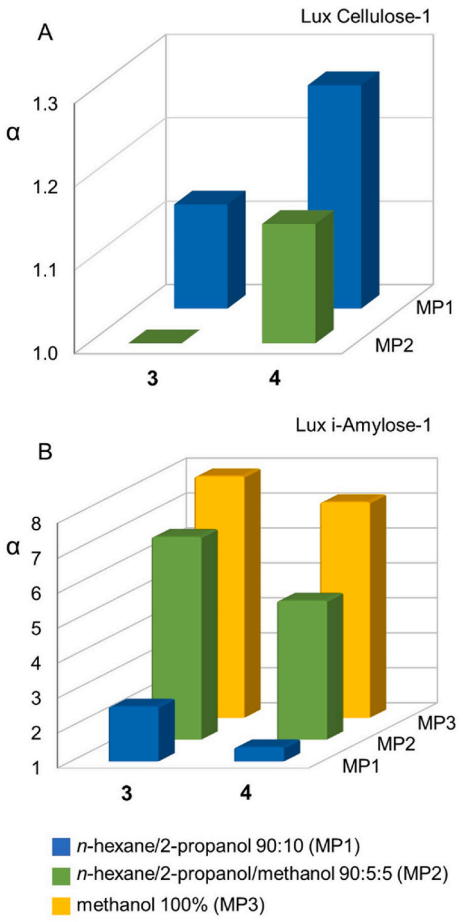

Fig. 5. Comparison of selectivity factor (α) of compounds **3** and **4** on Lux Cellulose-1 (A) and i-Amylose-1 (B) with *n*-hexane/2-propanol 90:10 v/v (MP1, blue), *n*-hexane/2-propanol/methanol 90:5:5 v/v/v (MP2, green), and pure methanol (MP3, yellow) as mobile phases (flow rate = 0.8 ml/min, T = 25 °C) (for chromatographic parameters see Table S3, Supplementary Data). (For interpretation of the references to colour in this figure legend, the reader is referred to the Web version of this article.)

compound **3** that was higher on the immobilized column. For both compounds **3** and **4**, selectivity (α) increased with the immobilized column compared to its coated version.

3. *Impact of chlorination on column selectivity.* Chlorination had a detrimental effect on α with the cellulose-based column, thus both compounds were unresolved with i-Cellulose-5. On the contrary, i-Amylose-3 showed higher α compared to i-Amylose-1, whereas retention factors decreased by changing i-Amylose-1 to i-Amylose-3.
4. *Impact of 2-PrOH content in the mobile phase.* By comparing the chromatographic parameters obtained in this study using *n*-hexane/2-PrOH 90:10 v/v with those obtained with the *n*-hexane/2-PrOH 95:5 v/v as mobile phase in our previous investigation [15], as expected, *k* and α decreased in all cases by increasing 2-PrOH content in the mobile phase, except for ferrocene **3** on Cellulose-1. In this case α increased from 1.08 (5 % 2-PrOH) to 1.13 (10 % 2-PrOH).

In a second screening, the effect of introducing MeOH in the mobile phase was considered by using *n*-hexane/2-PrOH/MeOH 90:5:5 v/v/v (MP2) and MeOH (MP3) as mobile phases, and *n*-hexane/2-PrOH 90:10 v/v (MP1) as reference for comparison with Lux Cellulose-1 and i-Amylose-1 as chiral columns (Fig. 5 and Supplementary data, Table S3). The addition of 5% MeOH to the *n*-hexane-based mobile phase had a detrimental effect on α for the enantioseparation of both **3** and **4** on Cellulose-1, whereas the use of MP2 and MP3 in place of MP1 increased retention and selectivity with the amylose-based chiral column.

The results of these screening confirmed that, although compounds **3** and **4** had structural similarity, different forces determined their retention and selectivity with the amylose-based selector compared to cellulose-based one. Indeed, for compound **4** the selectivity of enantioseparation was higher compared to the analogue **3** on the cellulose-based selector with all mobile phases, whereas the opposite behaviour was observed with the amylose-based chiral selector, and for compound **3** the enantioselectivity was higher compared to the analogue **4** with all mobile phases. Furthermore, on cellulose-based selector, selectivity decreased for both compounds by adding MeOH to the mobile phase. On the contrary, with the amylose-based chiral selector, strong noncovalent interactions enhanced the affinity of the second eluted (R_p)-enantiomers more than that of the first eluted (S_p)-enantiomers by adding MeOH to the mobile phase, even with small percentages in *n*-hexane-based mixtures. This effect was higher for **3** (MP2-MP1: $\Delta k_1 = 1.23$, $\Delta k_2 = 11.39$, $\Delta\alpha = 4.23$) compared to **4** ($\Delta k_1 = 0.11$, $\Delta k_2 = 4.71$, $\Delta\alpha = 3.57$). It is worth mentioning that, given the lower polarizability of MeOH (19.12 au) compared to *n*-hexane (72.80 au), the alcohol could exert lower competition for dispersion interactions than *n*-hexane [32], enhancing selector-analyte dispersion-type interactions.

3.2. Effect of temperature on the enantioseparation with n-hexane-based mobile phases

To gain further insights on the molecular bases of the observed chromatographic results, we explored analyte/CSP association based on thermodynamic considerations. In this study, we used van't Hoff equation (see Supplementary data for theory details) to determine the macroscopic thermodynamic quantities associated to the analyte transfer from the liquid phase to the CSP. Although deconvolution of the individual stereoselective and nonstereoselective interactions cannot be made by this procedure [33], its application to the enantioseparation of chemically related chiral analytes studied by systematically changing experimental conditions may provide reasonably reliable information on chiral recognition mechanisms [14,34].

Based on these considerations, retention and selectivity of compounds **3** and **4** on Cellulose-1, Amylose-1, i-Amylose-1, and i-Amylose-3 were determined at different temperatures from 5 to 45 °C in 5 °C increments by using *n*-hexane/2-PrOH 90:10 v/v as mobile phase (Supplementary data, Table S4). The thermodynamic quantities derived from van't Hoff plots (Figs. S5–S12) are reported in Table S5. As shown in Fig. 6, van't Hoff analysis explained the different chromatographic behaviour exhibited by compounds **3** and **4** on Cellulose-1 vs Amylose-1 in terms of different thermodynamics. For compound **3**, in the 5–45 °C temperature range, enantioseparation was entropy-driven on the Cellulose-1 ($\Delta\Delta H$, $\Delta\Delta S > 0$, $Q = 0.64$) and enthalpy-driven on the Amylose-1 ($\Delta\Delta H$, $\Delta\Delta S < 0$, $Q = 31.9$). In this latter case, a very low entropy penalty ($\Delta\Delta S = -0.05$ cal K^{-1} mol^{-1}) enhanced the enthalpy contribution ($\Delta\Delta H = -475.44$ cal mol^{-1}) to the difference between the free energy of adsorption of the two enantiomers ($\Delta\Delta G = -460.53$ cal mol^{-1}). On the contrary, enantioseparation of compound **4** was enthalpy-driven on Cellulose-1 ($\Delta\Delta H$, $\Delta\Delta S < 0$, $Q = 1.26$) and entropy-driven on Amylose-1 ($\Delta\Delta H$, $\Delta\Delta S > 0$, $Q = 0.82$). This trend confirmed the different interaction capability of compounds **3** and **4**, which behaved in a complementary manner between each other, as well as the complementary selectivity of Cellulose-1 vs Amylose-1 towards the two planar chiral ferrocenes.

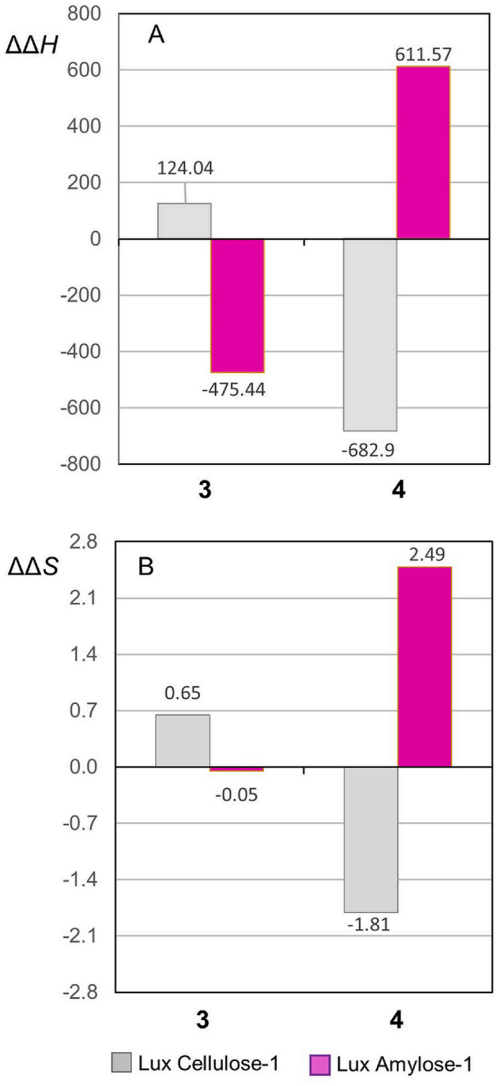

Fig. 6. Comparison of the $\Delta\Delta H$ (cal·mol^{-1}) and $\Delta\Delta S$ (cal·K^{-1}·mol^{-1}) terms contributing to the difference between the free energies of transfer of the two enantiomers from the mobile phase to the chiral stationary phase for compounds **3** and **4** on Lux Cellulose-1 (grey) and Amylose-1 (magenta), with *n*-hexane/2-propanol 90:10 v/v as mobile phase (flow rate = 0.8 ml/min) (for thermodynamic parameters see Table S5, Supplementary Data).

Furthermore, retention and selectivity of compounds **3** and **4** were determined at different temperatures from 5 to 45 °C in 5 °C increments by using *n*-hexane/2-PrOH/MeOH 90:5:5 v/v/v as mobile phase with Cellulose-1 and i-Amylose-1, and pure MeOH as polar organic mobile phase with the i-Amylose-1 exclusively (Supplementary data, Table S6). The thermodynamic quantities derived from van't Hoff plots (Figs. S13–S17) in these cases are reported in Table S7. All enantioseparations performed with the amylose-based column by using methanol-containing mobile phases were enthalpy driven. Higher $\Delta\Delta H$ were determined for compound **4** ($\Delta\Delta H = -1796.90$ and -2653.24 cal mol^{-1}) compared to **3** ($\Delta\Delta H = -1640.11$ and -1901.98 cal mol^{-1}). However, this enthalpy difference did not result in higher enantioselectivity for ferrocene **4** due to the higher entropy penalty ($\Delta\Delta S = -2.86$ and -5.02 cal K^{-1} mol^{-1}) observed for this compound compared to **3** ($\Delta\Delta S = -1.73$ and -2.30 cal K^{-1} mol^{-1}), reducing the difference between the free energy of adsorption of the two enantiomers. As a result, higher thermodynamic ratios were calculated for **3** ($Q = 3.18$, 2.77) compared to **4** ($Q = 2.11$, 1.77). The tendency toward higher values of $\Delta\Delta S$ determined for compound **3** could disclose higher disorder of the solvation shell around the amylose-based selector/**3** complexes compared to the amylose-based selector/**4** complexes because of the solvophobic effect favouring contacts between analyte and chiral selector surfaces. This trend was confirmed by comparing the entropy-enthalpy compensation (EEC) graphs collecting the thermodynamic quantities determined for **3** (Fig. 7A) and **4** (Fig. 7B) under the conditions mentioned above. In particular, the lower r^2 value associated with the trendline of the EEC graph of **3** ($r^2 = 0.867$) disclosed a higher mechanism variability compared to **4** ($r^2 = 0.954$). For ferrocene **3**, higher deviation from the linearity could be observed for the points (green square markers) related to the thermodynamic quantities associated with the use of i-Amylose-1 and MeOH-containing mobile phases. These observations could disclose the occurrence of a specific mechanism with (dispersion-type) forces of a different entity controlling enantiorecognition.

3.3. Effect of temperature on the enantioseparation with aqueous-organic mobile phases

The impact of solvation on dispersion forces is strongly dependent on solvent polarity. Recent studies highlighted that, in more polar solvents, solvophobic effects helped to stabilize dispersion forces, which was demonstrated by the addition of water to a polar organic solvent [32]. On this basis, to study the impact of increasing water content in MeOH and ACN as mobile phases, retention and selectivity of compounds **3** and **4** on i-Amylose-1 were determined at different temperatures from 10 to 60 °C in 5 °C increments by using the following mixtures as mobile phases: MeOH 100%, MeOH/H_2O 95:5 and 90:10 v/v (Supplementary data, Table S8, Table S9, and Fig. S18), ACN 100%, ACN/H_2O 90:10, 80:20, 70:30, and 60:40 v/v (Table S10, Table S11, and Fig. S19). The

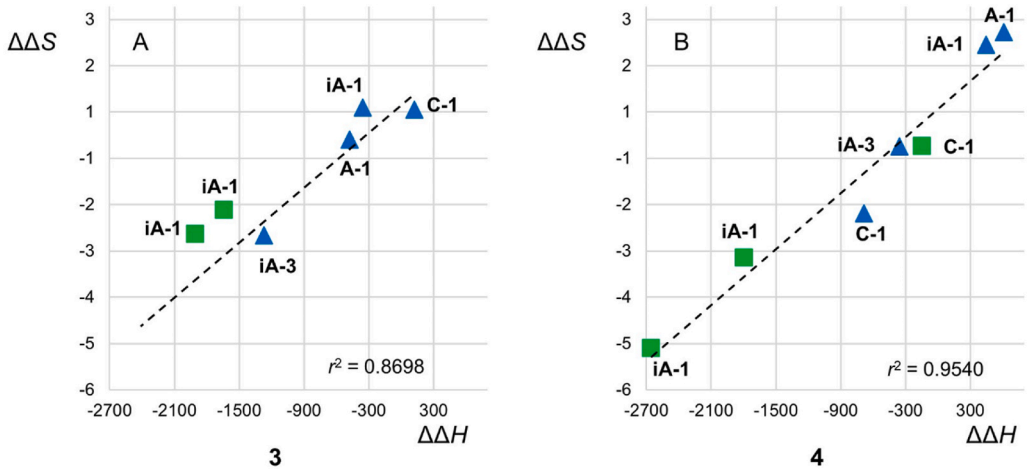

Fig. 7. Enthalpy-entropy compensation graphs [$\Delta\Delta H$ (cal·mol^{-1}) and $\Delta\Delta S$ (cal·K^{-1}·mol^{-1})] for compounds **3** and **4** with Lux Cellulose-1 (C-1), Amylose-1 (A-1), i-Amylose-1 (iA-1), and i-Amylose-3 (iA-3), as chiral columns, and *n*-hexane/2-propanol 90:10 v/v (blue markers), *n*-hexane/2-propanol/methanol 90:5:5 v/v/v and methanol 100 % as mobile phases (green markers) (flow rate = 0.8 ml/min) (for thermodynamic parameters see Tables S6 and S7, Supplementary Data). (For interpretation of the references to colour in this figure legend, the reader is referred to the Web version of this article.)

thermodynamic quantities derived from van't Hoff plots (Tables S12–S15, Figs. S20–S35) in these cases are reported in Tables 2–5.

It is worth noting that water has lower polarizability (5.74 au) than polar organic solvent like methanol (19.12 au) or acetonitrile (28.75 au), thus the dispersion energy donor capability of the bulk solvent is lower for water compared to methanol or acetonitrile. Consequently, enhancement of analyte-selector dispersion-type interaction could be expected by increasing water content. On the other hand, retention and selectivity also increased by increasing water content under reversed-phase conditions.

With aqueous MeOH mixtures as mobile phases, typical reversed-phase behavior was observed, and retention and selectivity increased as water concentration increased. For ferrocene **3**, the values of k_1 were always higher than those of ferrocene **4** at all temperatures and for each water percentage. On the contrary, for k_2 and α, the relative values of **3** and **4** were temperature- and water concentration-dependent. At 0 and 5% of water, k_2 was always higher for **3** compared to **4**. At 10 % concentration, k_2 was higher for **3** compared to **4** at T < 40 °C, whereas the opposite occurred at T ≥ 40 °C. In pure MeOH, α was higher for **3** than for **4** at all temperature, whereas the opposite could be observed at 5 and 10% water in MeOH. At higher water concentration and temperature, the following factors could cause the increase of k_2 and α for **4**:

1. At higher temperature, the conformational features of the selector may change [35], and the higher flexibility could enhance the penetration degree of the sterically hindered ferrocene **4.**
2. Higher temperature could increase the oscillation frequency of **4** molecular system [36], and consequently its vibrational frequency, enhancing its ability as dispersion energy donor.

In terms of thermodynamic parameters, the enantioseparations of **3** were enthalpy-driven in all cases, with a lower entropy penalty [$\Delta\Delta S = -1.31$ (5 % water) and 0.06 (10 % water)] and higher thermodynamic ratio [$Q = 4.05$ (5 % water) and 10.05 (10 % water)] compared to **4** ($-0.47 \leq \Delta\Delta S \leq -2.82$; $2.34 \leq Q \leq 9.92$).

ACN has higher polarizability compared to methanol, thus it exhibits higher bulk solvent competition in terms of dispersion-type interactions. In agreement with this hypothesis, lower *k* and α values were obtained with pure ACN and aqueous ACN mixtures, although typical reversed-phase behavior was observed, and retention increased as water concentration increased. On the contrary, addition of 10 % water in ACN substantially increased α values, whereas any further addition of water showed slight changes of selectivity. For *k*, the relative values of **3** and **4** were water content-dependent. Indeed, at lower percentages of water, *k* values were always higher for **3** compared to **4**, whereas the opposite trend could be observed at higher concentration of water. On the contrary, α values were higher for **3** compared to **4** in all cases.

All enantioseparations were enthalpy-driven, and the contribution of enthalpy to the differences of free energy related to the adsorption of the enantiomers increased as water concentration also increased due to a parallel decrease of the entropy penalty. However, a subtle difference was again observed between ferrocene **3** and **4**. For the 2-naphthyl derivative **4**, both $\Delta\Delta H$ and $\Delta\Delta S$ values decreased as water content in the mobile phase increased. For **3**, $\Delta\Delta H$ value increased as 10 % water was added to ACN, whereas it decreased for any further addition of water in the mobile phase.

These results showed that increasing temperature and water content in the mobile phase could increase the dispersion energy donor capability of the 2-naphthyl derivative **4**, smoothing the steric hindrance penalty responsible for the reduction of binding and enantiorecognition

Table 2
Thermodynamic parameters calculated from the van't Hoff plots (temperature range 283.15–333.15 K) for the enantioseparation of ferrocene **3** on Lux i-Amylose-1 with MeOH/H_2O 100:0, 95:5, and 90:10 v/v as MPs (flow rate = 0.8 ml/min).

Water%	enantiomer	ln *k* vs 1/T		ln *α* vs 1/T		
		ΔH (cal·mol^{-1})	ΔS^* (cal·K^{-1}·mol^{-1})	$\Delta\Delta H$ (cal·mol^{-1})	$\Delta\Delta S$ (cal·K^{-1}·mol^{-1})	T_{iso}, K (Q^a)
0	*S*	−2646.25 ± 93.1	−7.81 ± 0.30	−1575.94 ± 41.4	−1.31 ± 0.13	1207 (4.05)
	R	−4222.16 ± 126.8	−9.12 ± 0.41			
5	*S*	−2470.84 ± 186.3	−5.60 ± 0.61	−1328.98 ± 42.4	−0.44 ± 0.14	2996 (10.05)
	R	−3799.84 ± 209.80	−6.05 ± 0.68			
10	*S*	−2720.68 ± 153.8	−4.66 ± 0.50	−1198.20 ± 53.4	0.06 ± 0.17	–
	R	−3918.76 ± 134.6	−4.60 ± 0.44			

[a] $Q = \Delta\Delta H^\circ/(298.15 \times \Delta\Delta S^\circ)$, thermodynamic ratio.

Table 3
Thermodynamic parameters calculated from the van't Hoff plots (temperature range 283.15–333.15 K) for the enantioseparation of ferrocene **4** on Lux i-Amylose-1 with MeOH/H_2O 100:0, 95:5, and 90:10 v/v as MPs (flow rate = 0.8 ml/min).

Water%	enantiomer	ln *k* vs 1/T		ln *α* vs 1/T		
		ΔH (cal·mol^{-1})	Δ*S** (cal·K^{-1}·mol^{-1})	ΔΔ*H* (cal·mol^{-1})	ΔΔ*S* (cal·K^{-1}·mol^{-1})	T_{iso}, K (*Q*[a])
0	*S*	−1685.76 ± 32.9	−5.15 ± 0.11	−1972.81 ± 57.9	−2.82 ± 0.19	698 (2.34)
	R	−3658.51 ± 90.7	−7.97 ± 0.29			
5	*S*	−2121.00 ± 96.9	−4.79 ± 0.14	−1593.67 ± 66.4	−1.26 ± 0.22	992 (4.24)
	R	−3714.69 ± 99.8	−6.05 ± 0.32			
10	*S*	−2258.43 ± 112.0	−3.29 ± 0.36	−1400.98 ± 44.3	−0.47 ± 0.14	2957 (9.92)
	R	−3659.39 ± 153.3	−3.76 ± 0.50			

[a] $Q = \Delta\Delta H^{\circ}/(298.15 \times \Delta\Delta S^{\circ})$, thermodynamic ratio.

Table 4
Thermodynamic parameters calculated from the van't Hoff plots (temperature range 283.15–333.15 K) for the enantioseparation of ferrocene **3** on Lux i-Amylose-1 with ACN/H_2O 100:0, 90:10, 80:20, 70:30, and 60:40 v/v as MPs (flow rate = 0.8 ml/min).

Water%	enantiomer	ln *k* vs 1/T		ln *α* vs 1/T		
		ΔH (cal·mol^{-1})	Δ*S** (cal·K^{-1}·mol^{-1})	ΔΔ*H* (cal·mol^{-1})	ΔΔ*S* (cal·K^{-1}·mol^{-1})	T_{iso}, K (*Q*[a])
0	*S*	−2028.73 ± 120.6	−7.12 ± 0.39	−1450.57 ± 27.8	−2.09 ± 0.09	694 (2.33)
	R	−3479.10 ± 145.5	−9.21 ± 0.47			
10	*S*	−2240.06 ± 229.5	−7.25 ± 0.75	−1585.88 ± 46.2	−1.67 ± 0.15	950 (3.18)
	R	−3825.83 ± 241.4	−8.92 ± 0.79			
20	*S*	−2689.52 ± 174.4	−7.04 ± 0.57	−1424.07 ± 109.3	−1.14 ± 0.36	1249 (4.19)
	R	−4113.65 ± 127.8	−8.18 ± 0.42			
30	*S*	−2070.89 ± 96.8	−3.36 ± 0.31	−1431.09 ± 59.4	−1.27 ± 0.19	1127 (3.78)
	R	−3502.05 ± 118.8	−4.63 ± 0.39			
40	*S*	−1626.91 ± 150.7	−0.45 ± 0.49	−1388.58 ± 66.37	−1.20 ± 0.22	1157 (3.88)
	R	−3015.47 ± 209.82	−1.64 ± 0.68			

[a] $Q = \Delta\Delta H^{\circ}/(298.15 \times \Delta\Delta S^{\circ})$, thermodynamic ratio.

Table 5
Thermodynamic parameters calculated from the van't Hoff plots (temperature range 283.15–333.15 K) for the enantioseparation of ferrocene **4** on Lux i-Amylose-1 with ACN/H_2O 100:0, 90:10, 80:20, 70:30, and 60:40 v/v as MPs (flow rate = 0.8 ml/min).

Water%	enantiomer	ln *k* vs 1/T		ln *α* vs 1/T		
		ΔH (cal·mol^{-1})	Δ*S** (cal·K^{-1}·mol^{-1})	ΔΔ*H* (cal·mol^{-1})	ΔΔ*S* (cal·K^{-1}·mol^{-1})	T_{iso}, K (*Q*[a])
0	*S*	−2040.45 ± 48.3	−7.31 ± 0.16	−1508.39 ± 75.4	−2.53 ± 0.24	596 (2.00)
	R	−3548.86 ± 118.5	−9.84 ± 0.39			
10	*S*	−1995.74 ± 130.6	−6.51 ± 0.42	−1482.16 ± 85.3	−1.67 ± 0.28	887 (2.98)
	R	−3477.91 ± 211.8	−8.17 ± 0.69			
20	*S*	−2850.13 ± 301.5	−7.45 ± 0.98	−1248.15 ± 99.9	−0.83 ± 0.32	1504 (5.04)
	R	−4098.25 ± 233.3	−8.28 ± 0.76			
30	*S*	−1900.71 ± 67.3	−2.51 ± 0.22	−1173.45 ± 27.1	−0.66 ± 0.09	1778 (5.96)
	R	−3074.19 ± 92.3	−3.18 ± 0.30			
40	*S*	−1333.44 ± 142.2	1.02 ± 0.46	−1165.76 ± 59.6	−0.68 ± 0.19	1714 (5.75)
	R	2.499.21 ± 201.0	0.34 ± 0.65			

[a] $Q = \Delta\Delta H^{\circ}/(298.15 \times \Delta\Delta S^{\circ})$, thermodynamic ratio.

at lower temperature and low content of water.

3.4. Effect of substituents introduced in 1-(iodoethynyl)-3-phenylferrocene

We extended our investigation under chromatographic conditions to the derivatives of the phenyl iodoethynyl ferrocene **3** bearing methyl (**5**) or *t*-butyl (**6**) group at the 4-position of the phenyl ring. It is worth mentioning that a recent theoretical study confirmed the higher strength of *t*-butyl and phenyl groups as dispersion energy donors compared to the methyl group and demonstrated high dispersion energy donor capability for iodine and acetylene groups as well [22]. Furthermore, by comparing the crystal packing of the (*S*)-enantiomers of compounds **3**, **5** and **6**, the presence of the *t*-Bu groups in compound **6** induced a highly ordered crystal packing consisting of motifs interacting together through multiple H···C contacts (Supplementary data, Fig. S3). The same type of close contacts could be observed for compound **3** [28] in the solid state, but not for compound **5** (Fig. S2) bearing the Me group on the phenyl ring.

Although crystal compression could favour close H···C contacts, and noncovalent interactions in the solid state may be different compared to those observed in solution, higher capability as dispersion energy donor could be envisaged for **6** compared to **5** in solution considering their different features in terms of crystal packing. Moreover, dispersion interactions involving *t*-butyl groups were demonstrated to occur in solution by experimental and computational studies [22,37].

The enantioseparation of compounds **5** and **6** was explored by using i-Amylose-1 as chiral column, *n*-hexane/2-PrOH 95:5 v/v and *n*-hexane/2-PrOH/MeOH 95:2.5:2.5 v/v/v as mobile phases. The enantioseparation parameters collected for **3** under these elution conditions were used as reference for comparison (Fig. 8 and Supplementary data, Fig. S36 and Table S16). We noted that the presence of a substituent on the aromatic ring was detrimental for the high affinity of compound **3** toward the amylose-based CSP, likely due to steric effect limiting the penetration of the analyte into the amylose selector groove. On this basis, k_1 and k_2 values changed following the order **3** > **5** > **6** by using *n*-hexane/2-

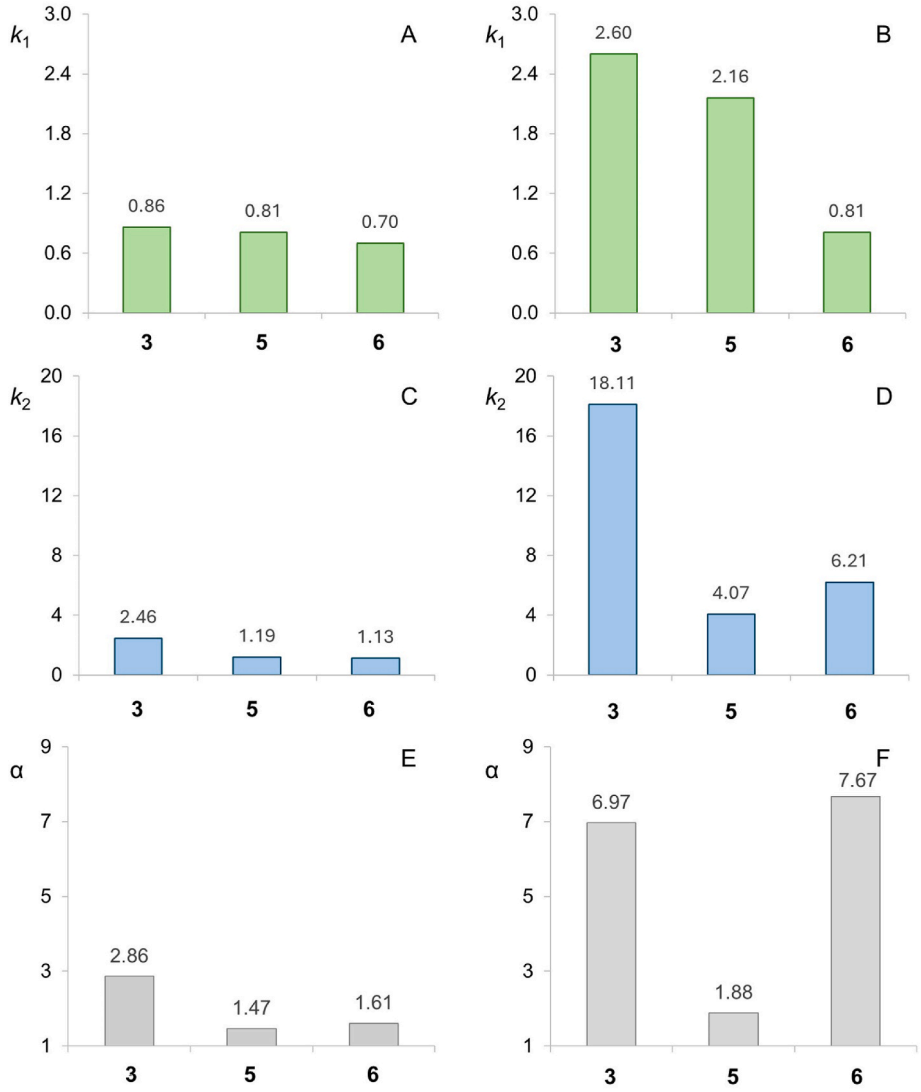

Fig. 8. Comparison of retention factors of first (k_1) (S_p) and of second (k_2) (R_p) eluted enantiomers, and selectivity (α) of compounds **3** (R = H═), **5** (R = Me), and **6** (R = *t*-Bu) on Lux i-Amylose-1 with *n*-hexane/2-propanol 95:5 v/v (A, C, E) and *n*-hexane/2-propanol/methanol 95:2.5:2.5 v/v/v (B, D, F) (flow rate = 0.8 ml/min, T = 25 °C) (see Fig. S36 and Table S16 in Supplementary Data for chromatographic traces and parameters).

PrOH 95:5 v/v as mobile phase [EEO = (S_p)-(R_p)]. Thus, under these conditions the steric hindrance controlled the affinity of the enantiomers for the chiral selector. However, whereas k_2 decreased substantially from **3** to **5** ($\Delta k_2 = 1.27$), very low decrease was observed by moving from **5** to **6** ($\Delta k_2 = 0.06$). This data showed that even in the absence of methanol in the mobile phase, other attractive forces opposed to the steric hindrance, resulting in slightly higher selectivity determined for **6** (α = 1.61) compared to **5** (α = 1.47) by using the *n*-hexane/2-PrOH mixture as mobile phase. As expected, this effect was even more evident with the methanol-containing mobile phase. In this case, the second eluted (R_p)-enantiomer of the *t*-butyl substituted ferrocene **6** showed higher affinity (k_2 = 6.21) toward the CSP compared to the corresponding (R_p)-enantiomer of the methyl substituted derivative (k_2 = 4.07), resulting in higher α value (α = 7.67) compared to that of **5** (α = 1.88) and even to that of ferrocene **3** (α = 6.97).

4. Conclusions

Although it is a commonly accepted opinion that dispersion forces are attenuated in solvent media, recent theoretical and experimental studies showed that dispersion forces may contribute to aromatic stacking even in polarizable organic solvent [38]. Nevertheless, experimental confirmation for the dominance of dispersion forces in aromatic stacking, in alkyl···alkyl, and in alkyl···aromatic interactions occurring in organic solution remains rather limited. This is caused by the fact that dispersion forces are strongly molecular system- and distance-dependent, as well as strongly dependent on medium polarizability and size of the interacting surfaces [32]. In this regard, identifying dispersion forces in enantioseparation science is a challenging task which deserves to be tackled for two reasons: a) the role of dispersion forces is less studied in enantioseparation science, and b) the chromatographic system is particularly versatile to study dispersion forces given that several pivotal factors like structure of the interacting molecules, medium (mobile phase) composition and temperature can be easily varied. For this purpose, amylose-based chiral selectors appeared very versatile due to their compact structure. On the other hand, the extended surface featuring these polymeric selectors may favour the large changes in the involved interacting surfaces upon binding that are needed for identifying dispersion-driven contacts through measurable energy changes. Furthermore, based on van der Waals potential, there is a subtle distance-dependent balance between steric effects and London dispersion, thus subtle changes in size and geometry of the system can impact dispersion forces. These reasons may justify why unusual affinity of the enantiomers was sometimes observed on the more compact

amylose-based selectors compared to the looser cellulose-based polymers.

Based on these considerations, our study reasonably confirmed that dispersion-type forces may be involved in binding and enantiorecognition occurring in chromatographic environment. The main results of this study can be summarized as follows:

1) At temperature below 40 °C and in non-aqueous mobile phases, ferrocene **3** showed better ability as dispersion energy donor compared to **4.**
2) Boundary parameters affecting enantioseparation outcomes, like temperature and mobile phase composition, could be modulated to enhance dispersion-type forces, attenuating the impact of the steric hindrance on the strength of shorter contacts. This was observed in the case of ferrocene **4.**
3) Solvent polarizability affected the capability of the bulk solvent as dispersion energy donor competing with selector and analyte, thus attenuating, or suppressing analyte-selector dispersion-type contacts. On these bases, given the solvent polarizability increasing in the order water < methanol < ACN ≪ *n*-hexane, higher retention for the second eluted (R_p)-enantiomers and in most cases for selectivity was observed for **3** and **4** following the opposite order water > methanol > ACN ≫ *n*-hexane.
4) In the case of 1-(iodoethynyl)-3-(4-*t*-butyl)phenylferrocene **6**, higher k_2 and α values were observed compared to the 4-methyl-substituted derivative **5** with the amylose *tris*(3,5-dimethylphenyl)carbamate-based column in MeOH-containing mobile phase.

These results demonstrated that in liquid-phase enantioseparation steric repulsion can be turned into (dispersion) attraction depending on the features of analyte, polysaccharide selector, and mobile phase.

CRediT authorship contribution statement

Barbara Sechi: Writing – review & editing, Formal analysis, Data curation. **Nutsa Tsetskhladze:** Writing – review & editing, Data curation. **Luke Connell:** Data curation. **Alessandro Dessì:** Writing – review & editing, Formal analysis. **Roberto Dallocchio:** Writing – review & editing, Formal analysis. **Bezhan Chankvetadze:** Writing – review & editing, Resources. **Sergio Cossu:** Writing – review & editing, Data curation. **Tamar Khatiashvili:** Writing – review & editing, Data curation. **Victor Mamane:** Writing – review & editing, Project administration, Funding acquisition. **Paola Peluso:** Writing – review & editing, Writing – original draft, Project administration, Methodology, Funding acquisition, Formal analysis, Conceptualization.

Declaration of competing interest

The authors declare that they have no known competing financial interests or personal relationships that could have appeared to influence the work reported in this paper.

Data availability

Data will be made available on request.

Acknowledgements

Open Access funding provided by Consiglio Nazionale delle Ricerche (CNR) within the CRUI-CARE agreement. We thank CNR (Grant no.: SAC. AD002.011.032) and SRNSFG (Shota Rustaveli National Science Foundation of Georgia) (Grant no.: CNR-22-259) for the Italy-Georgia Joint Bilateral Agreement, and the University of Strasbourg, the Centre National de la Recherche Scientifique (CNRS), and the French National Research Agency (Grant no.: ANR-21-CE07-0014) for financial support.

Appendix A. Supplementary data

Supplementary data to this article can be found online at https://doi.org/10.1016/j.aca.2024.343160.

References

[1] P. Peluso, B. Chankvetadze, Recognition in the domain of molecular chirality: from noncovalent interactions to separation of enantiomers, Chem. Rev. 122 (2022) 13235–13400, https://doi.org/10.1021/acs.chemrev.1c00846.
[2] P. Peluso, B. Chankvetadze, Fundamentals of enantioselective liquid chromatography, in: S. Fanali, B. Chankvetadze, P.R. Haddad, C.F. Poole, M.-L. Riekkola (Eds.), Liquid Chromatography: Fundamentals and Instrumentation, third ed., Vol 1, Elsevier, Amsterdam, 2023, pp. 383–439, https://doi.org/10.1016/B978-0-323-99968-7.00024-2.
[3] M. Lämmerhofer, Chiral recognition by enantioselective liquid chromatography: mechanisms and modern chiral stationary phases, J. Chromatogr. A 1217 (2010) 814–856, https://doi.org/10.1016/j.chroma.2009.10.022.
[4] G.K.E. Scriba, Chiral recognition in separation sciences. Part I: polysaccharide and cyclodextrin selectors, Trends Anal. Chem. 120 (2019) 115639, https://doi.org/10.1016/j.trac.2019.115639.
[5] G.K.E. Scriba, Chiral recognition in separation sciences. Part II: macrocyclic glycopeptide, donor-acceptor, ion-exchange, ligand-exchange and micellar selectors, Trends Anal. Chem. 119 (2019) 115628, https://doi.org/10.1016/j.trac.2019.115628.
[6] P. Peluso, V. Mamane, R. Dallocchio, A. Dessì, S. Cossu, Noncovalent interactions in high-performance liquid chromatography enantioseparations on polysaccharide-based chiral selectors, J. Chromatogr. A 1623 (2020) 461202, https://doi.org/10.1016/j.chroma.2020.461202.
[7] E.F. Pettersen, T.D. Goddard, C.C. Huang, G.S. Couch, D.M. Greenblatt, E.C. Meng, T.E. Ferrin, UCSF Chimera–A visualization system for exploratory research and analysis, J. Comput. Chem. 25 (2004) 1605–1612, https://doi.org/10.1002/jcc.20084.
[8] B. Chankvetadze, Recent developments on polysaccharide-based chiral stationary phases for liquid-phase separation of enantiomers, J. Chromatogr. A 1269 (2012) 26–51, https://doi.org/10.1016/j.chroma.2012.10.033.
[9] P. Peluso, B. Chankvetadze, The molecular bases of chiral recognition in 2-(benzylsulfinyl)benzamide enantioseparation, Anal. Chim. Acta 1141 (2021) 194–205, https://doi.org/10.1016/j.aca.2020.10.050.
[10] P. Peluso, V. Mamane, E. Aubert, A. Dessì, R. Dallocchio, A. Dore, P. Pale, S. Cossu, Insights into halogen bond-driven enantioseparations, J. Chromatogr. A 1467 (2016) 228–238, https://doi.org/10.1016/j.chroma.2016.06.007.
[11] P. Peluso, A. Dessì, R. Dallocchio, B. Sechi, C. Gatti, B. Chankvetadze, V. Mamane, R. Weiss, P. Pale, E. Aubert, S. Cossu, Enantioseparation of 5,5'-dibromo-2,2'-dichloro-3-selanyl-4,4'-bipyridines on polysaccharide-based chiral stationary phases: exploring chalcogen bonds in liquid-phase chromatography, Molecules 26 (2021) 221, https://doi.org/10.3390/molecules26010221.
[12] P. Peluso, B. Sechi, G. Lai, A. Dessì, R. Dallocchio, S. Cossu, E. Aubert, R. Weiss, P. Pale, V. Mamane, B. Chankvetadze, Comparative enantioseparation of chiral 4,4'-bipyridine derivatives on coated and immobilized amylose-based chiral stationary phases, J. Chromatogr. A 1625 (2020) 461303, https://doi.org/10.1016/j.chroma.2020.461303.
[13] P. Vaňkátová, A. Kubíčková, K. Kalíková, How mobile phase composition and column temperature affect enantiomer elution order of liquid crystals on amylose tris(3-chloro-5-methylphenylcarbamate) as chiral selector, Electrophoresis 42 (2021) 1844–1852, https://doi.org/10.1002/elps.202000350.
[14] B. Sechi, A. Dessì, R. Dallocchio, N. Tsetskhladze, B. Chankvetadze, M. Pérez-Baeza, S. Cossu, G. Jibuti, V. Mamane, P. Peluso, Unravelling dispersion forces in liquid-phase enantioseparation. Part I: impact of ferrocenyl versus phenyl groups, Anal. Chim. Acta 1278 (2023) 341725, https://doi.org/10.1016/j.aca.2023.341725.
[15] A. Dessì, B. Sechi, R. Dallocchio, B. Chankvetadze, M. Pérez-Baeza, S. Cossu, V. Mamane, P. Pale, P. Peluso, Comparative enantioseparation of planar chiral ferrocenes on polysaccharide-based chiral stationary phases, Chirality 34 (2022) 609–619, https://doi.org/10.1002/chir.23417.
[16] P. Peluso, V. Mamane, R. Dallocchio, A. Dessì, R. Villano, D. Sanna, E. Aubert, P. Pale, S. Cossu, Polysaccharide-based chiral stationary phases as halogen bond acceptors: a novel strategy for detection of stereoselective σ-hole bonds in solution, J. Separ. Sci. 41 (2018) 1247–1256, https://doi.org/10.1002/jssc.201701206.
[17] P.R. Schreiner, Dispersion interactions, Beilstein J. Org. Chem. 14 (2018) 3076–3077, https://doi.org/10.3762/bjoc.14.286.
[18] S. Grimme, Dispersion interaction and chemical bonding, in: G. Frenking, S. Shaik (Eds.), The Chemical Bond - Chemical Bonding across the Periodic Table, John Wiley and Sons, Weinheim, 2014, pp. 477–478.
[19] D. Yepes, F. Neese, B. List, G. Bistoni, Unveiling the delicate balance of steric and dispersion interactions in organocatalysis using high-level computational methods, J. Am. Chem. Soc. 142 (2020) 3613–3625, https://doi.org/10.1021/jacs.9b13725.
[20] C. Eschmann, L. Song, P.R. Schreiner, London dispersion interactions rather than steric hindrance determine the enantioselectivity of the Corey–Bakshi–Shibata reduction, Angew. Chem. Int. Ed. 60 (2021) 4823–4832, https://doi.org/10.1002/anie.202012760.
[21] G. Gryn'ova, C. Corminboeuf, Steric "attraction": not by dispersion alone, Beilstein J. Org. Chem. 14 (2018) 1482–1490, https://doi.org/10.3762/bjoc.14.125.

[22] E. Solel, M. Ruth, P.R. Schreiner, London dispersion helps refine steric A-values: dispersion energy donor scales, J. Am. Chem. Soc. 143 (2021) 20837–20848, https://doi.org/10.1021/jacs.1c09222.
[23] S.-S. Sun, Peptide folding driven by Van der Waals interactions, Protein Sci. 24 (2015) 1383–1388, https://doi.org/10.1002/pro.2710.
[24] C. Cantatore, M. Korb, H. Lang, R. Cirilli, ON/OFF receptor-like enantioseparation of planar chiral 1, 2-ferrocenes on an amylose-based chiral stationary phase: the role played by 2-propanol, Anal. Chim. Acta 1211 (2022) 339880, https://doi.org/10.1016/j.aca.2022.339880.
[25] S. Grimme, Do special noncovalent π-π stacking interactions really exist? Angew. Chem. Int. Ed. 47 (2008) 3430–3434, https://doi.org/10.1002/anie.200705157.
[26] R.J. Durand, S. Achelle, S. Gauthier, N. Cabon, M. Ducamp, S. Kahlal, J.-Y. Saillard, A. Barsella, F. Robin-Le Guena, Incorporation of a ferrocene unit in the π-conjugated structure of donor-linker-acceptor (D-π-A) chromophores for nonlinear optics (NLO), Dyes Pigments 155 (2018) 68–74, https://doi.org/10.1016/j.dyepig.2018.03.029.
[27] A.H. Heindl, R.C. Wende, H.A. Wegner, London dispersion as important factor for the stabilization of (Z)-azobenzenes in the presence of hydrogen bonding, Beilstein J. Org. Chem. 14 (2018) 1238–1243, https://doi.org/10.3762/bjoc.14.106.
[28] V. Mamane, P. Peluso, E. Aubert, R. Weiss, E. Wenger, S. Cossu, P. Pale, Disubstituted ferrocenyl iodo- and chalcogenoalkynes as chiral halogen and chalcogen bond donors, Organometallics 39 (2020) 3936–3950, https://doi.org/10.1021/acs.organomet.0c00633.
[29] H. Koller, K.E. Rimböck, A. Mannschreck, High-pressure liquid chromatography on triacetylcellulose: characterization of a sorbent for the separation of enantiomers, J. Chromatogr. A 282 (1983) 89–94, https://doi.org/10.1016/S0021-9673(00)91594-2.
[30] Gaussian 16, Revision C.01, M.J. Frisch, G.W. Trucks, H.B. Schlegel, G.E. Scuseria, M.A. Robb, J.R. Cheeseman, G. Scalmani, V. Barone, G.A. Petersson, H. Nakatsuji, X. Li, M. Caricato, A.V. Marenich, J. Bloino, B.G. Janesko, R. Gomperts, B. Mennucci, H.P. Hratchian, J.V. Ortiz, A.F. Izmaylov, J.L. Sonnenberg, D. Williams-Young, F. Ding, F. Lipparini, F. Egidi, J. Goings, B. Peng, A. Petrone, T. Henderson, D. Ranasinghe, V.G. Zakrzewski, J. Gao, N. Rega, G. Zheng, W. Liang, M. Hada, M. Ehara, K. Toyota, R. Fukuda, J. Hasegawa, M. Ishida, T. Nakajima, Y. Honda, O. Kitao, H. Nakai, T. Vreven, K. Throssell, J.A. Montgomery Jr., J.E. Peralta, F. Ogliaro, M.J. Bearpark, J.J. Heyd, E.N. Brothers, K.N. Kudin, V.N. Staroverov, T.A. Keith, R. Kobayashi, J. Normand, K. Raghavachari, A.P. Rendell, J.C. Burant, S.S. Iyengar, J. Tomasi, M. Cossi, J.M. Millam, M. Klene, C. Adamo, R. Cammi, J.W. Ochterski, R.L. Martin, K. Morokuma, O. Farkas, J.B. Foresman, D. J. Fox, Gaussian, Inc., Wallingford CT, 2016.
[31] A.V. Marenich, C.J. Cramer, D.G. Truhlar, Universal solvation model based on solute electron density and a continuum model of the solvent defined by the bulk dielectric constant and atomic surface tensions, J. Phys. Chem. B 113 (2009) 6378–6396, https://doi.org/10.1021/jp810292n.
[32] L.-A. Gravillier, S.L. Cockroft, Context-dependent significance of London dispersion, Acc. Chem. Res. 56 (2023) 3535–3544, https://doi.org/10.1021/acs.accounts.3c00625.
[33] A. Sepsey, An adventurous journey around the thermodynamics of liquid chromatography, LCGC North Am. 40 (2022) 584–586, https://doi.org/10.56530/lcgc.na.qk2090y9.
[34] D. Tanács, T. Orosz, Z. Szakonyi, T.M. Le, F. Fülöp, W. Lindner, I. Ilisz, A. Péter, High-performance liquid chromatographic enantioseparation of isopulegol-based ß-amino lactone and ß-amino amide analogs on polysaccharide-based chiral stationary phases focusing on the change of the enantiomer elution order, J. Chromatogr. A 1621 (2020) 461054, https://doi.org/10.1016/j.chroma.2020.461054.
[35] I. Matarashvili, G. Kobidze, A. Chelidze, G. Dolidze, N. Beridze, G. Jibuti, T. Farkas, B. Chankvetadze, The effect of temperature on the separation of enantiomers with coated and covalently immobilized polysaccharide-based chiral stationary phases, J. Chromatogr. A 1599 (2019) 172–179, https://doi.org/10.1016/j.chroma.2019.04.024.
[36] Z. Gong, H. Sun, B.E. Eichinger, Temperature transferability of force field parameters for dispersion interactions, J. Chem. Theor. Comput. 14 (2018) 3595–3602, https://doi.org/10.1021/acs.jctc.8b00104.
[37] H.-J. Schneider, Distinction and quantification of noncovalent dispersive and hydrophobic effects, Molecules 29 (2024) 1591, https://doi.org/10.3390/molecules29071591.
[38] L. Yang, J.B. Brazier, T.A. Hubbard, D.M. Rogers, S.L. Cockroft, Can dispersion forces govern aromatic stacking in an organic solvent? Angew. Chem. Int. Ed. 55 (2016) 912–916, https://doi.org/10.1002/anie.201508056.